J. Fluid Mech. (1991), vol. 226, pp. 219–242
Printed in Great Britain

An optical interferometric study of the wake of a bluff body

By R. B. GREEN AND J. H. GERRARD
Department of Engineering, University of Manchester, Manchester M13 9PL, UK

(Received 6 February 1989 and in revised form 29 October 1990)

A Fizeau optical interferometer has been used to visualize the wake behind a circular cylinder at low Reynolds numbers Re. As well as showing the vortex shedding mechanism and development of the far wake in a new light, the shed vortex strength and age were derived from the results. The vortex velocity distributions, at downstream distances of 5 to 16 diameters, were found to be those of convected Oseen vortices. These measurements confirmed the existence of a transition at $Re \approx 100$, which reflects the emergence of convection as the dominant process in the near wake.

1. Introduction

Vortex shedding from a bluff body is a well-documented subject. As the Reynolds number (Re) is increased from zero to several million the flow, and the wake in particular, undergoes a multitude of transitional phenomena which are mostly not of the classical laminar to turbulent type. The existence of a transition at $Re \approx 100$ has been a hotly debated issue. The contention was between a transition in the vortex shedding mechanism (Tritton 1954) and the effects of the onset of three-dimensionalities (Gaster 1971). There followed extended exchanges involving many authors essentially on the question of whether or not there was a discontinuity in the frequency – Re relationship. This culminated in Williamson (1989) clearly showing that such discontinuities are attributable to three-dimcnsional effects. He has shown that a discontinuity at $Re \approx 64$ marks the change from parallel to slantwise shedding of vortices. He also discovered a frequency transition at $170 \leqslant \mathrm{Re} \leqslant 180$ associated with streamwise vortex elements. It is noteworthy that in the towing tank used by Gerrard (1978) vortex loops exactly like those in figure 3 of Williamson's 1988 paper were (later) found to be formed at $Re > 100$ and so a frequency discontinuity at $Re \approx 100$ would be expected.

The controversy that existed over the possible existence of a shedding frequency transition did, however, bring to light other more fundamental transitional phenomena at $Re \approx 100$. Gerrard (1978) noticed that there was a discontinuity in the time taken for a vortex to accelerate to its final velocity at $Re \approx 100$. Slaouti (1980) observed an increase in the rate of scavenging of fluid out of the near wake above $Re = 100$. Most importantly Gerrard (1978) indicated that there was evidence for a strong transition in the shed vortex strength at $Re = 100$. The plot of the dimensionless vortex strength as a function of Re shown in his paper is reproduced in figure 1. In this figure, points 1 and 3 are due to Thom (1933), who used a hot-wire technique to find shedding frequency and vortex spacing, vortex strength then being calculated directly from these. Point 2 is due to Schaefer & Eskinazi (1959), point 4

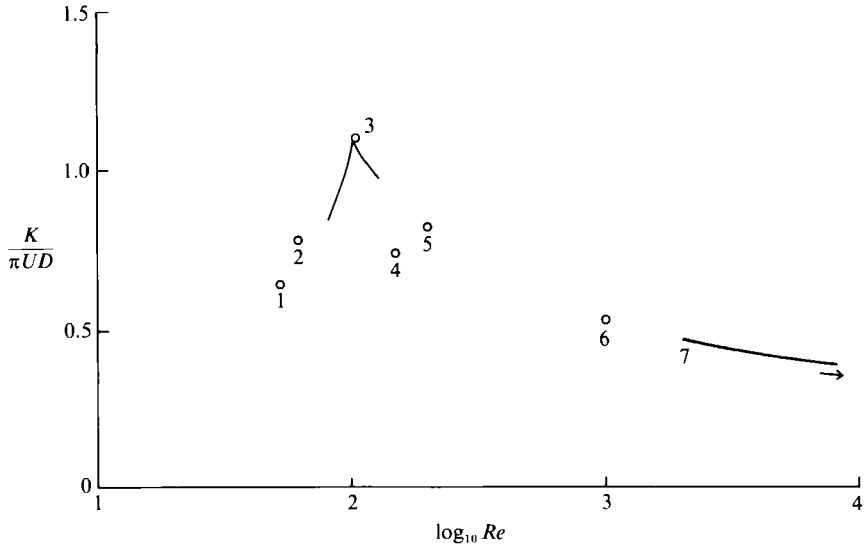

FIGURE 1. Variation of vortex strength with Re using data currently available. Points 1 and 3 are due to Thom (1933), point 2 to Schaefer & Eskinazi (1959), point 4 to Berger (1964), points 5 and 6 to Timme (1957) and line 7 to Bloor & Gerrard (1966). The solid lines around point 3 are the results of the present work.

to Berger (1964) and line 7 to Bloor & Gerrard (1966). All these workers used hot-wire techniques to measure wake velocity profiles and a wake model to convert these measurements into vortex strengths. Points 5 and 6 are due to Timme (1957) who measured velocity in the wake by photographing the motions of aluminium particles floating on a water surface. The velocity measurements were then fitted to a vortex model. Schmidt & Tilman (1972) measured vortex strength in the range $5460 < Re < 128000$ using an ultrasound technique and obtained good agreement with Bloor & Gerrard (1966). The transition in the vortex strength is expected to be reflected in the amplitude of the oscillating lift and drag coefficients. Measurements of oscillating lift and drag are scarce, though the results of Tanida, Okajima & Watanabe (1973) might suggest that the lift coefficient has a maximum at $Re = 100$ while the drag coefficient has a minimum at the same Re. Unfortunately, they presented only four measurements of lift and drag in the range $60 < Re < 120$, and made no comment on the behaviour of C_L and C_D around $Re = 100$. Unal & Rockwell (1988) present measurements of the amplitude of streamwise oscillating velocity at $Re \geqslant 100$ which, like the base suction, peaks at $Re \approx 200$.

It is the primary objective of the present study to find the variation of vortex strength with Reynolds number. The curve with a peak at $Re = 100$ on figure 1 is a result of the present work. In the present method an optical interferometric method of measurement of the surface deformation in the wakes of circular cylinders is used. The cylinders were towed through water with their axes vertical. In §2 the water surface deformation induced by an Oseen vortex is presented. The interferometer and its use is described in §§3 and 4. Section 5 shows the results of flow visualization using the interferometer while §6 contains a description of the method of determination of vortex strength and age (or size of the core of the vortex) from the water surface deformation. A more extended account is given by Green (1989). We have not attempted the solution of the general problem of the determination of the

pressure from a measured surface shape knowing the surface tension. Besides this being a difficult problem its solution does not lead directly to the vortex strength. Evidence from flow visualization (e.g. Gerrard 1978), from numerical analysis (e.g. Benson *et al.* 1989) and from the application of particle tracking methods in which the vorticity can be determined from the velocity field (Green 1989) shows that close to the cylinder the vortices are not axisymmetric, but become so some 5 diameters downstream of body. It will be shown in the present work that beyond this distance downstream the vortices possess an Oseen vortex distribution. Strength and age of the vortex were varied to obtain a match between the calculated and measured surface shape. That the results obtained at a fixed Reynolds number are independent of the cylinder diameter shows that the method is reliable. The accuracy falls off at large distances downstream because the number of fringes associated with a vortex decreases. Particular care has been taken to ensure that the background disturbance level is only about one fringe, corresponding to a surface height change of 316.4 nm.

2. The water surface deformation caused by a vortex

Slaouti & Gerrard (1981) found that if a circular cylinder was towed along a water tank with its axis penetrating the surface normally, then the shed vortices would also penetrate the surface normally if the surface had been cleared of all contaminants. Furthermore, for the same water surface condition, shed vortices would still penetrate the surface normally if the top of the cylinder was below the water surface provided the distance between the top of the cylinder and the water surface (the gap size) was less than one fifth of a cylinder diameter. If the vortex penetrates the water surface normally, then the pressure distribution across the vortex will deform the water surface, the exact shape of the water surface being governed by the vortex properties. The flow at the surface is locally two-dimensional and is effectively at the centre of a cylinder of twice the actual length below the water surface. The following is an account of how a suitable method for measuring the water surface deformation caused by a bluff body wake was developed, the intention being some means of determining shed vortex strength.

2.1. *Basic theory*

At Reynolds numbers of the order of 100, shed vortices can be accurately modelled by Oseen vortices. This has been done successfully in the past – see, for example, Schaefer & Eskinazi (1959). Slaouti (1980) carried out some basic theoretical work to determine the water surface depression caused by an Oseen vortex. The following outlines the main points.

The Oseen vortex is best represented by its velocity distribution

$$V_\theta = \frac{K}{2\pi r}\left(1-\exp\left(\frac{-r^2}{4\nu t}\right)\right), \tag{1}$$

where K is the vortex strength or circulation, t is the vortex age, ν the kinematic viscosity and r the distance from the axis of the vortex at which V_θ is being determined. The pressure gradient in an axisymmetric flow is given by

$$\frac{\partial p}{\partial r} = \frac{\rho V_\theta^2}{r}, \tag{2}$$

where p is the pressure and ρ the fluid density.

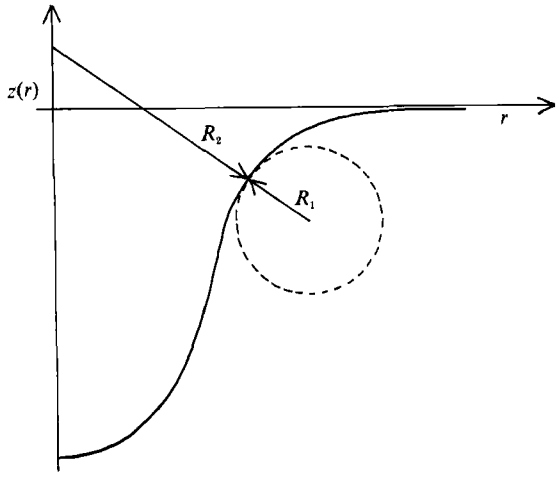

FIGURE 2. Curvature of an axisymmetric surface. R_1 is the plane radius of curvature and R_2 is the axisymmetric radius of curvature.

The pressure difference distribution $\Delta p(u)$ (which is simply $p_\infty - p(u)$, p_∞ being the pressure at $r = \infty$) is found by substituting (1) into (2) and integrating the result. This gives

$$\Delta p(u) = \rho k^2 (E(u) - E(2u) + \frac{(1-\exp(-u))^2}{2u} \tag{3}$$

where $u = r^2/4\nu t$ and

$$E(u) = \int_u^\infty \frac{\exp(-x)\partial x}{x}$$

2.2. *The effect of surface tension*

When a water surface is distorted, surface tension acts to minimize the surface area. This is achieved by a pressure jump δp through the water surface, which is given by

$$\delta p = \gamma k, \tag{4}$$

where γ is the surface tension and k is the water surface curvature. For an axisymmetric surface, k is given by

$$k = \frac{1}{R_1} + \frac{1}{R_2}, \tag{5}$$

where R_1 and R_2 are the principal radii of curvature (see Daly 1969). The two senses of curvature are shown in figure 2 and are both perpendicular to the surface at the point under consideration.

R_1 is the plane radius of curvature and is given by

$$R_1 = \frac{(1+z'(r)^2)^{\frac{3}{2}}}{z''(r)}, \tag{6}$$

where z is the vertical coordinate of the water surface. The effect of the surface tension pressure associated with this component of curvature is to reduce the amplitude of deformation of the water surface.

R_2 is the axisymmetric radius of curvature and is given by

$$R_2 = \frac{(1+z'(r)^2)^{\frac{1}{2}}r}{z'(r)}. \tag{7}$$

The effect of this component is to pull the surface towards the z-axis.

If it is assumed that $z'^2 \ll 1$ then the complete expression for the surface tension pressure is given by

$$\Delta p = \gamma\left(z''(r)+\frac{z'(r)}{r}\right). \tag{8}$$

2.3. *The complete equation for the water deformation and its solution*

The pressure distribution required to produce a water surface profile $z(r)$ is equal to the gravitational component plus the surface tension component. In this case the pressure distribution is caused by an Oseen vortex and, therefore, the complete expression for the water surface deformation is given by

$$z''(r)+\frac{z'(r)}{r}-Cz(r) = B\left(E(u)-E(2u)+\frac{(1-\exp(-u))^2}{2u}\right) \tag{9}$$

where $C = \rho g/\gamma$ and $B = \rho K^2/16\pi\nu t\gamma$

To solve (9) the boundary conditions at $r = 0$ are used – these are as follows:

$z(0) = -A$, the maximum depression which is unknown.

$z'(0) = 0$, the gradient of the depression at the origin which must be zero.

$z''(0)$ is unknown but must be determined.

It follows that by studying the limits of (9) as $r \to 0$ then

$$z''(0) = \tfrac{1}{2}(B\ln 2 - AC).$$

Thus there is one unknown, the maximum water surface depression A.

Since the pressure difference a long way from the vortex axis must approach zero, then as $r \to \infty$, $z(r) \to 0$. This boundary condition can be used to determine A and hence $z(r)$. A suitable method of solution involves iterating the value of A to find the value that gives a monotonic increase in $z(r)$ to zero as $r \to \infty$. Vortex age and strength are treated as known quantities. Equation (9) was solved numerically using the Runge–Kutta method and thus the pressure can be obtained from the surface depression with surface tension included. Surface tension typically reduced the depression at the centre by a factor of three and increased the radius of the depression. The surface depression at the vortex was typically about 10 μm. This is very important in dictating the design of an instrument suitable for finding vortex strength by measuring water surface deformation. The following section outlines the design of such an instrument.

3. An optical interferometer suitable for measuring small water surface displacements

A suitable technique for measuring water surface displacements of the order of 10 μm was required. To measure free surface displacements of about this size in a vial of rotating liquid helium, Marston & Fairbank (1977) used an optical interferometer which showed contours of constant surface height. Slaouti (1980) concluded that

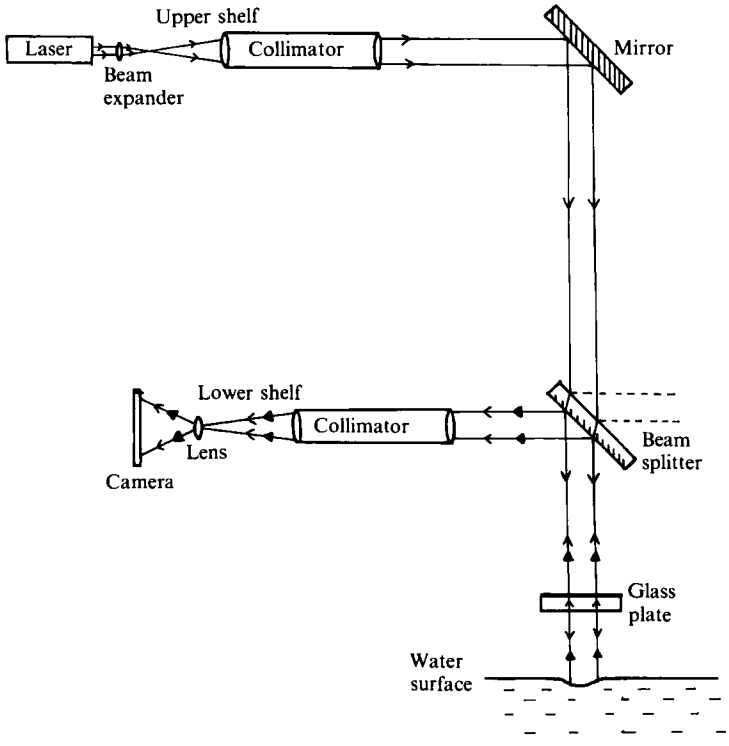

FIGURE 3. The water tank interferometer. The top surface of the glass plate has an anti-reflection coating.

such an instrument would be suitable for measuring small water surface displacements in the wake of a bluff cylinder. It is interesting to note that contours of surface height were published by Eisner (1929) from stereoscopic photographs of the waves produced by a towed body. Such a technique requires very extensive data reduction. A brief description of the apparatus follows. A full description can be found in Green (1989).

3.1. *Design of the Interferometer*

The interferometer was derived from the Fizeau type and is sketched in figure 3. Figure 4 shows the interferometer and the towing tank. The mirrors and lenses were arranged to produce and photograph the interference effect between coherent wave fronts reflected from the water surface and the lower surface of the glass plate. The top surface of the plate carried a non-reflective coating.

3.2. *The design of the towing tank for use with the interferometer*

The essential features included in the design of the water tank and model towing system were as follows. Background motion in the tank was kept to a minimum. For this the Perspex tank had a well fitting lid, double glazing on the sides and was placed on top of an insulation-filled cavity. The towing system produced as closely as possible a constant vibration-free towing speed. Vibration levels were less than 0.5% of cylinder speed which was more constant than this. The effect of ground-borne vibrations was minimized by supporting the tank on a sturdy frame which was mounted on partly inflated pneumatic tyres. A stiff cantilever framework reaching

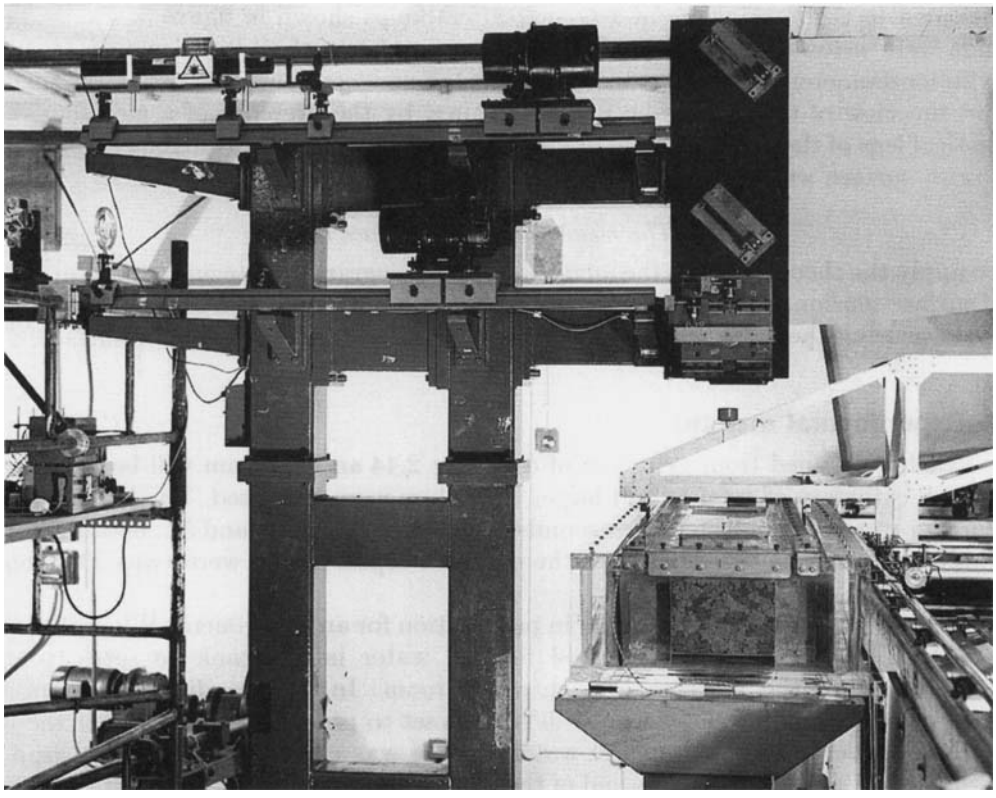

FIGURE 4. Interferometer, water tank, model support framework and towing carriage.

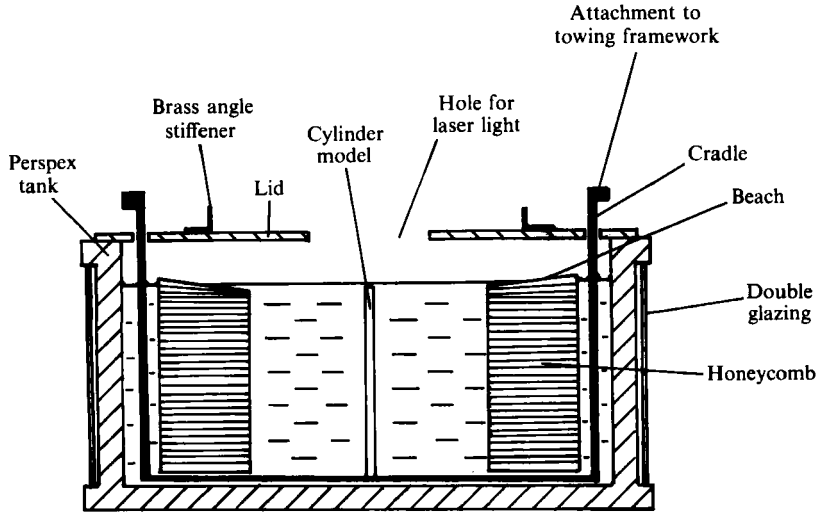

FIGURE 5. Cross-section of the water tank at the working section showing the arrangement of the beaches and the U-shaped cradle.

out over the tank was attached to the towing carriage. Cylinder models were attached to the lower plate of a U-shaped cradle as shown in figure 5. Their upper ends were below the water surface with a gap of less than $0.2D$, where D is the cylinder diameter. In this condition the axes of vortices penetrate the water surface and the view of the near wake is not obscured by the presence of a meniscus. The vertical legs of the cradle ran outside a beach and honeycomb arrangement placed to absorb surface waves and sloshing motions.

3.3. *The measurement of surface tension*

To apply the theory of §2 to the analysis of interferograms, an accurate measurement of surface tension is necessary. The surface tension of the water in the tank was found by measuring the force required to lift a thin metal ring off the water surface.

4. Experimental method

Results obtained from cylinders of diameter 2.44 and 3.02 mm will be presented, though cylinders of smaller and larger diameters were also used. The length of the cylinder was 157 mm which corresponds to aspect ratios of 64 and 52: because of the water surface boundary condition the effective aspect ratios were twice the above values.

A careful procedure was followed in preparation for an experiment. When the tank was refilled, one week was allowed for the water in the tank to settle to the temperature of the temperature-controlled room. In this condition background motions were minimized. The water level was set to produce a small gap at the top of the cylinder. Before a run the water surface was cleaned by placing a drop of detergent on the surface at one end of the tank and sucking debris away at the other. Three hours were allowed for the associated disturbances to die away. In the meantime, the rails, the wheels, and their bearings were cleaned and polished and checked for smooth running. Just prior to the run the glass plate was levelled to give as few fringes as possible (typically two) across the field of view. The run could then proceed and a rapid sequence of photographs was taken when the cylinder entered the field of view after about 1.5 m of travel down the tank. Surface tension was measured immediately after the run.

5. Interferogram results

Interferograms were recorded on Kodak Tri-X 400 ASA film. To enhance fringe contrast, the films were under-exposed and over-developed, the required exposure depending on the magnification used. The results for cylinder diameters of 2.44 mm and 3.02 mm only will be shown. All distances quoted are measured from the rear surface of the cylinder.

5.1. *Interpretation of the interferograms*

Figure 6 shows an interferogram for a Reynolds number of 80.0 with a cylinder diameter of 3.02 mm. The cylinder is just visible on the photograph but is outlined with a dashed circle for clarity. The large, dark disc to the right of the cylinder is a marker used to locate the cylinder. The cylinder motion is from the bottom to the top of the picture. The dark, straight bands running across the picture are a diffraction pattern produced by a thin fiducial wire placed over the collimator on the lower shelf.

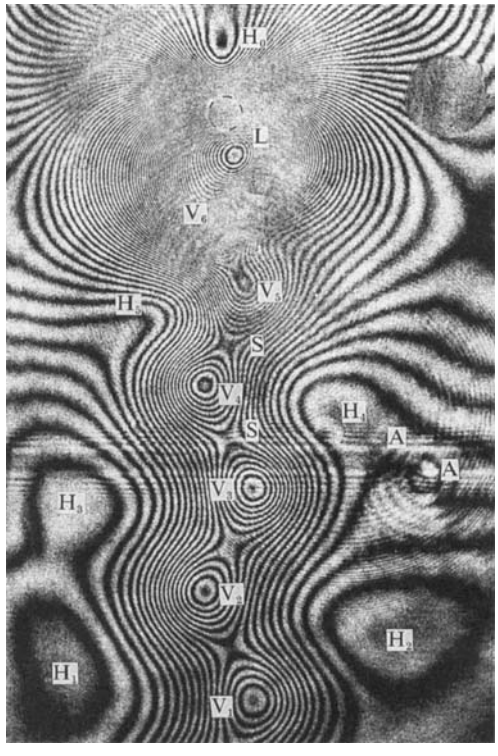

FIGURE 6. Interferogram showing near wake and far wake for $Re = 80.0$, $D = 3.02$ mm.

The faint concentric circles centred around the positions marked A on the middle right of the picture are diffraction patterns caused by lens aberrations. A similar structure can be seen between the positions marked L and V_6.

Cylinder vibration results in the blurred region surrounding the cylinder on figure 6 and on the other interferograms. The interferogram requires interpretation since isolated depressions and hills look alike. A fringe is a contour of constant surface height which cannot cross other contours and cannot end without discontinuous changes in surface height. The height difference between two dark or two bright fringes is equivalent to a surface height difference of half a wavelength of laser light, or 316.4 nm. The complicated structure of the interferograms shown in figures 6 and 7 can be explained in terms of the vortex wake. The largest elevations and depressions marked H_0 and L respectively on the figures are close to the cylinder. As we will describe below, the centre of the low-pressure region L oscillates in position. The low pressure is produced by the curvature of the streamlines flanking this region. In front of the body the high-pressure region H_0 is associated with stagnation at the front of the body. This region stands away from the cylinder because of the effect of surface tension and flow over the top of the cylinder. These regions would be made invisible by the meniscus if the body passed through the water surface. With a small gap between the water surface and the top of the cylinder these regions are visible but no attempt has been made to quantify their magnitude or exact position in the absence of surface tension effects.

The development of the near wake can be seen on figure 6 and more clearly in figure 7. The fringes around the centre of the low-pressure region L are stretched

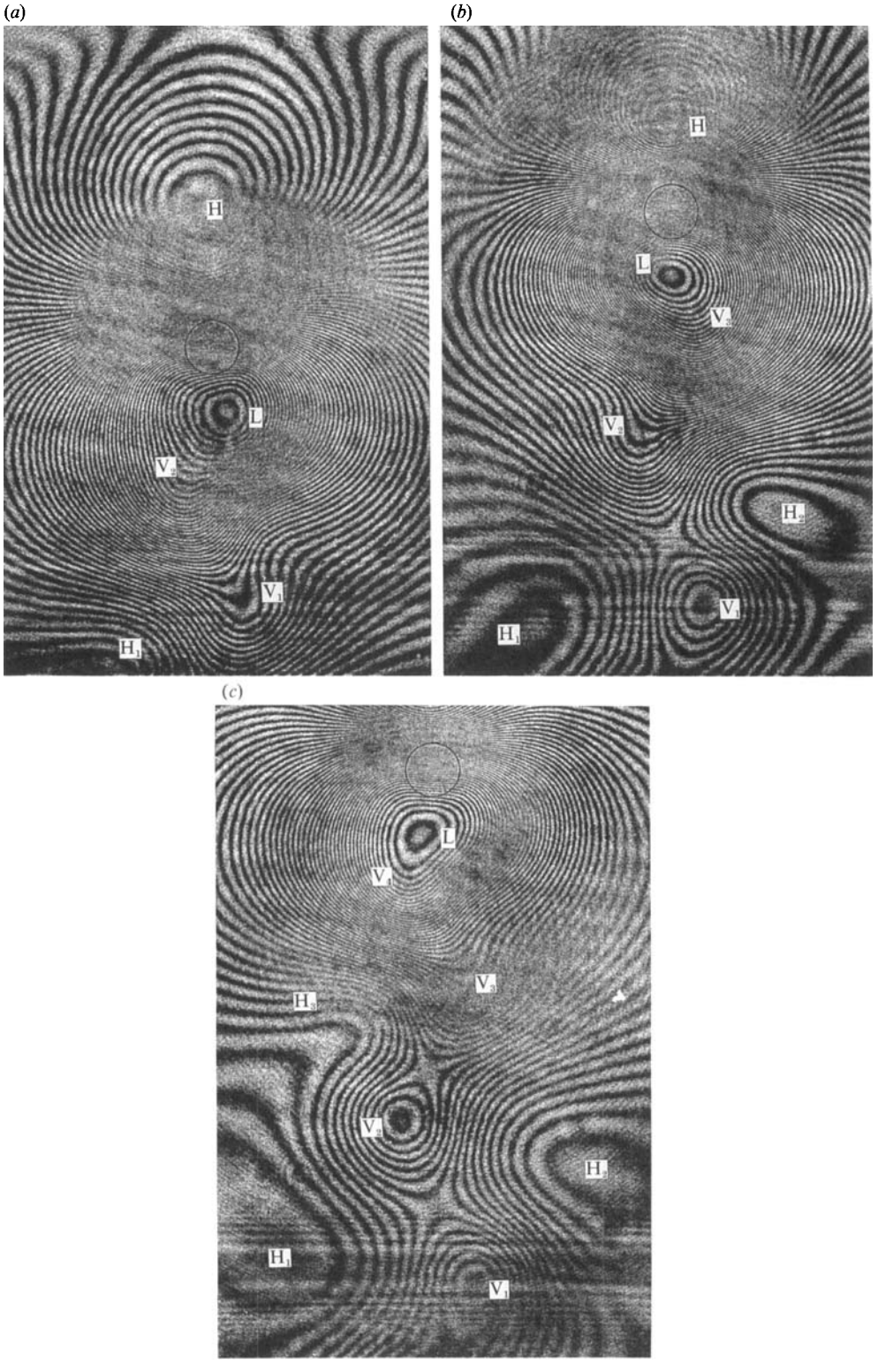

FIGURE 7 (*a–c*). Sequence of interferograms showing the near wake for $Re = 80.3$, $D = 3.02$ mm. The time difference between successive frames is 0.41 shedding periods.

towards the bottom left in figure 7 (*a*). Referring back to figure 6, in the region V_6 the first vortex is forming and the low pressure extends into this region. A similar low-pressure area is associated with the second vortex at V_5 which is seen as a valley in the side of the main depression. Further downstream, individual more isolated vortices V_4 and V_3 etc. appear. Between these, saddle points marked S can be seen. The fringe passing through a saddle point is referred to as a separatrix fringe. In the region H_5 there is a spur of a hill marking a region of higher pressure. High-pressure regions marked H in figure 6 occur on each side of the vortex wake and are located opposite vortices on the other side of the vortex sheet. These high-pressure regions are the result of the translational motion of the vortex street through the fluid. The relative velocity of the street and the surrounding fluid drops to zero opposite the vortices on the far side of the street.

5.2. *Description of the shedding cycle*

A sequence of pictures at $Re = 80.3$ with a cylinder of diameter 3.02 mm was taken. Figure 7 (*a–c*) shows the shedding cycle and some subsequent development of the street, there being just less than one half of the shedding cycle between each picture. Again the cylinder is moving from the bottom to the top of the picture.

In figure 7 (*a*) the depression L is at about $x/D = 1$ and is displaced to the right. The following frame, figure 7 (*b*), shows the centre of L to be in line with the cylinder axis and the direction of motion of the cylinder, though it is now extended to the bottom right (region V_3) indicating the presence of a vortex there. In the previous frame, figure 7 (*a*), the dimple was extended towards the bottom left (shown as V_2) – this has developed into the region V_2 of low water surface gradient (i.e. a vortex) at $x/D = 4$ and to the left of L in figure 7 (*b*). Thus, one sees in figure 7 the valley on the side of the depression L develop into discrete fringe centres as the vortices are shed and pass downstream.

A video camera was used to observe the shedding cycle in greater detail. The low-pressure centre L was observed to stay on one side of the cylinder for about four fifths of that half of the shedding cycle. Consider the case of the centre L initially being on the right of the cylinder. A decreased gradient first appears ahead of the centre on the other side of the cylinder. The dimple then rapidly slides (in about one tenth of the cycle) across the wake onto the left side and is now extended to the bottom right. The asymmetry gradually moves further away until it can be seen as a region of higher fringe spacing. The main depression remains relatively unchanged except that it moves very slightly away from the cylinder until it elongates slightly to the top right and then rapidly moves across to the right. The centre of the depression then repeatedly executes this figure-of-eight motion. Therefore, it is the growth of a structure on one side of the wake that precedes the shedding of a vortex on the other side of the wake. Good descriptions of the shedding cycle obtained by dye or smoke flow visualisation may be found in Slaouti (1980) and Freymuth, Finaish & Bank (1986).

5.3. *Comparison of interferograms with results of previous work*

Although the wake of a bluff body has not been investigated using this technique before, various works are available for comparison. Pressure contours from a solution of the Navier–Stokes equations at $Re = 100$ were obtained by Braza *et al.* (private communication, based on the work of Braza, Chassaing & Ha Minh 1986) and are shown in figure 8 (*a–d*). These results may be compared with figures 7 (*a–c*) at $Re = 80.3$ since we found no change in the appearance of the near wake with Reynolds number. The pressure contours from the work of Braza *et al.* show regions of

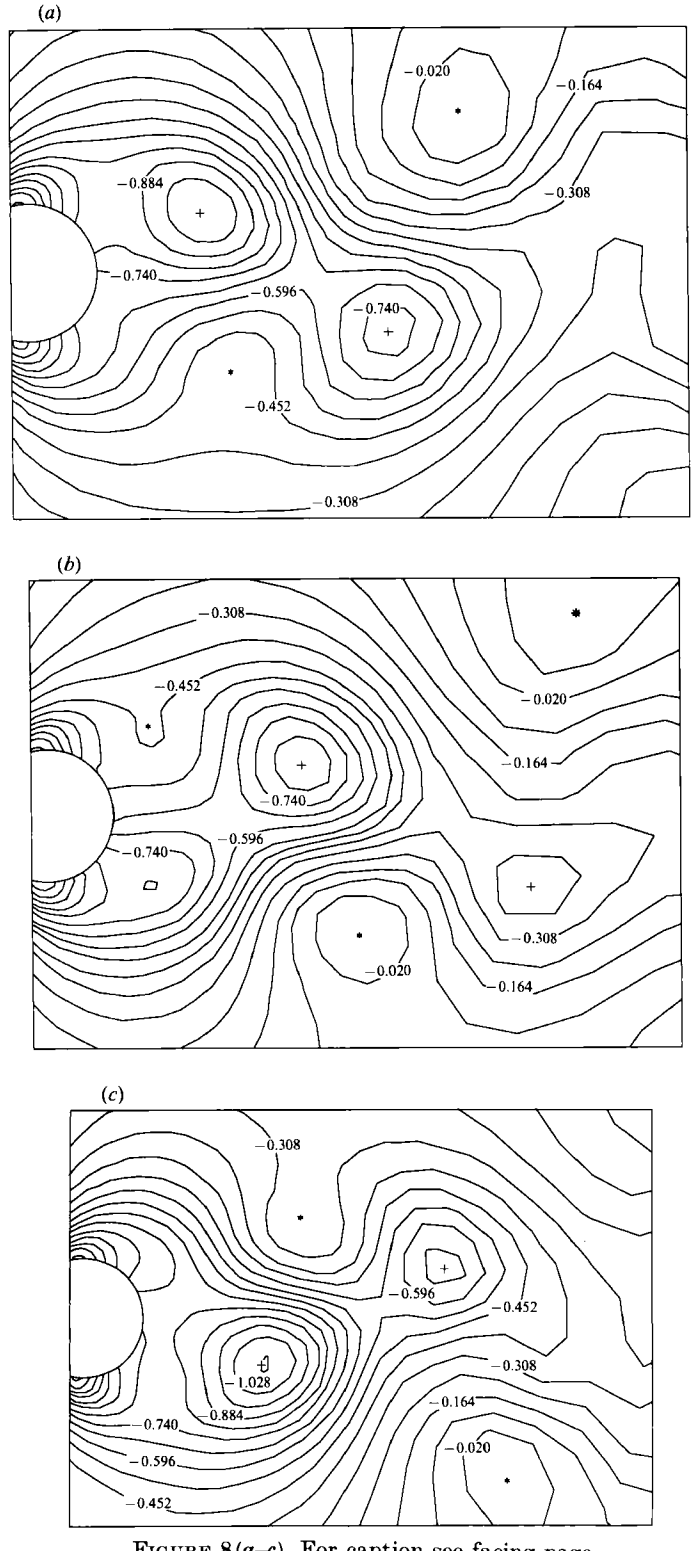

FIGURE 8(*a–c*). For caption see facing page.

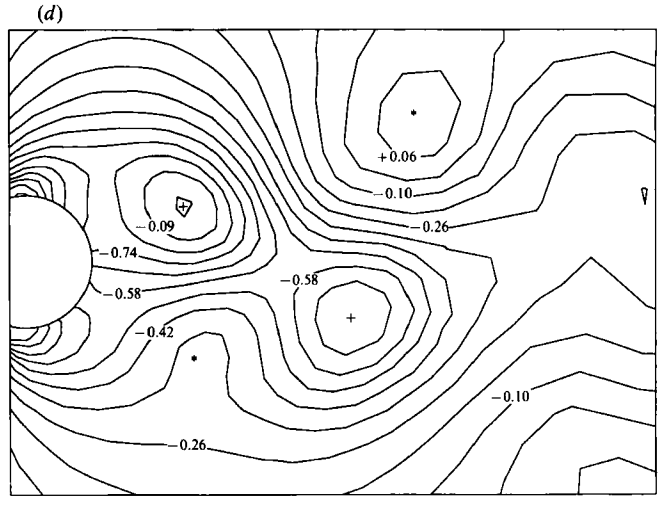

FIGURE 8. Pressure contours in the near wake of a circular cylinder at $Re = 100$ obtained from a solution of the Navier–Stokes equations (Braza *et al.* private communication, based on the work of Braza *et al.* 1986). The time difference between successive figures is one third of a shedding period. (*a*) $T = 50$, (*b*) $T = 54.18$, (*c*) $T = 58.36$, (*d*) $T = 62.54$. There is a difference in C_p of 0.072 between each contour in (*a*), (*b*) and (*c*) and a difference of 0.080 in (*d*).

low pressure, indicated by a +, and regions of high pressure, indicated by a * on opposite sides of the wake. Such regions of high and low pressure were inferred from the interferograms in the above discussion. The value of the minimum pressure at the centre of each vortex becomes less negative as the vortex moves away from the cylinder, corresponding with the decrease in maximum depression of a shed vortex with increasing x/D in the interferograms. A major difference between the surface height contours and the pressure contours, however, is the appearance of the contours around the cylinder. Agreement in this region is not expected because of the action of surface tension and the large surface height changes close to the cylinder. The numerical results of Braza *et al.* (figures 8*a–d*) indicate that the minimum pressure lies behind the cylinder and not at the cylinder surface, so the centre of the main dimple in an interferogram can be taken as the position of minimum pressure in the wake. The exact position of the minimum pressure shown by Braza *et al.* oscillates in a similar way to the motion of the low-pressure region in the interferograms. Pressure measurements in the wake made by Roshko (1954) showed that the minimum pressure for a circular cylinder at $Re = 14500$ lies at about $0.5\,D$ behind the back of the cylinder, a phenomenon he attributed to the vortex formation processes; it is likely that this is the reason for the minimum pressure lying about $1\,D$ behind the back of the cylinder at $Re = 100$.

The behaviour of the far wake can be compared with velocity measurements in the wake taken by, for example, Cimbala, Nagib & Roshko (1988). The decrease in maximum depression and increase in fringe spacing shown in figure 6 indicates weakening and/or diffusion of the shed vortices. The decrease in wake oscillating velocity with distance behind the cylinder found by Cimbala *et al.* (1988) reflects this change. Note that flow visualization by conventional means (e.g. Gerrard 1978, who used dye, or Zdravkovitch (1969) who used smoke) can be misleading; it is the present rate of rotation of dye or smoke that indicates the vortex properties and not the persistence of the dye or smoke pattern. This was a problem discussed by Cimbala

et al. (1988). In this respect, flow visualization using the interferometer offers the advantage of showing vortex strength directly. It does need to be stressed, however, that far downstream the vortices do still rotate though very slowly. This rotation and interaction between the vortices results in secondary and tertiary vortex streets of larger scale (Taneda 1959; Honji 1986).

6. Inference of vortex strength from an interferogram

The problem of finding the vortex strength and age can be attacked in various ways. It is reasonable to assume that the age is increasing monotonically with distance behind the cylinder. Schaefer & Eskinazi (1959) extended this relationship by assuming that the age was proportional to the distance behind the cylinder, i.e. vortices were diffusing as if they were isolated. This relationship is over-simplified if the vortices are diffusing into one another causing weakening, which may result in some redistribution of vorticity. A method of finding vortex age from the geometry of the vortex street is also likely to be unreliable owing to the unpredictable nature of the vortex paths – vortex paths are anything but repeatable. It must be noted that vortex age is a measure of the size of the vortex and is therefore not zero at the time of the first appearance of a vortex on an interferogram. A suitable method of finding strength and age from an interferogram involves comparing water surface profiles caused by Oseen vortices (using the results of §2) with water surface profiles shown by an interferogram. This matching requires justification because neighbouring vortices have overlapping velocity fields, the effect of which has to be shown to be small. We will show that the vorticity fields of adjacent vortices overlap by only a small amount. The effect of the velocity field is illustrated in figure 9. We consider the distributions along lines perpendicular to the wake centreline on opposite sides of the vortex street. The pressure change produced by the neighbouring vortices is different on the two sides of the vortex and changes sign between the inside and outside of the street. All the distributions obtained were compared on the two sides of the vortex and it was found that the two profiles always differed in the expected sense and by an insignificant amount (less than one fringe). Along the transverse line it was also found that the fringe displacement from the background level (zero height change) is only about one fringe at a distance from the vortex equal to the separation between adjacent vortices. This shows that the vortex pressure distribution is close to that of the Oseen vortex and that the uncertainty is one fringe or less.

It is possible in principle to determine pressures from interferograms in the non-axisymmetric case. This would require a determination of the principle radii of curvature at each point; the attendant inaccuracies would be expected to be large. This procedure, however, does not lead directly to vortex strength. Integration of the vorticity obtained from differentiating the measured velocity field is the (in this case less accurate) direct method of vortex strength determination. This we have done (Green 1989) and will publish separately.

Water surface profiles measured from the interferograms at $Re = 84.1$ with a cylinder diameter of 2.44 mm are shown in figure 10. The vertical scale is expressed as the number of fringes F above the vortex centre. The profiles become flatter and more extended with distance behind the cylinder owing to diffusion and weakening of the vortices. Comparisons between different runs with the same cylinder at the same Reynolds number produced excellent repeatability (better than one fringe) between water surface profiles even though the vortex paths may have been very different. Inaccuracy of measurement of the distance of a fringe away from the

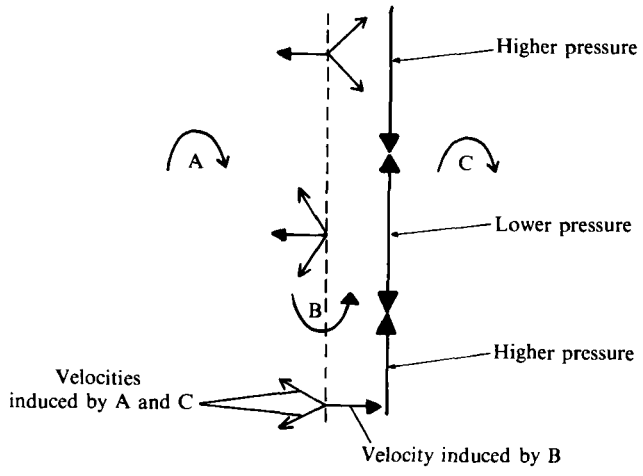

FIGURE 9. Effect of neighbouring vortices on pressure field of Vortex B. Regions of higher or lower pressure as a result of the effect of neighbouring vortices are indicated.

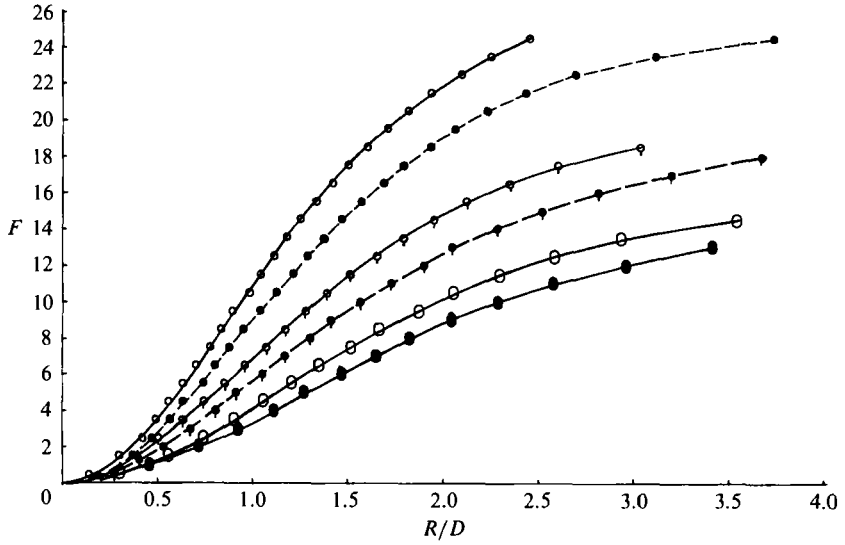

FIGURE 10. Variation of experimental water surface deformations with x/D at $Re = 84.1$. The units of depth are half-wavelengths of laser light or 316.4 nm. $D = 2.44$ mm. ○, $x/D = 5.2$; ●, $x/D = 8.0$; ♀, $x/D = 10.8$; ♀, $x/D = 13.5$; 0, $x/D = 16.3$; ♀, $x/D = 19.2$.

vortex centre is shown by the slight waviness in each surface profile. Vortex strengths and ages were then found from a water surface profile by getting as close a match as possible between an Oseen vortex profile and an experimental one. Important results of the theory in §2 are that for a given vortex age, the water surface depression at a given R/D is proportional to strength squared, and that for a given vortex strength, the water surface gradient at a given R/D decreases with increasing age. (R is distance from the vortex centre.) The matching process therefore involved iterating the vortex age and was as follows:

(i) Two points on the experimental profile were chosen – usually at $R/D = 1$ and 2.5.

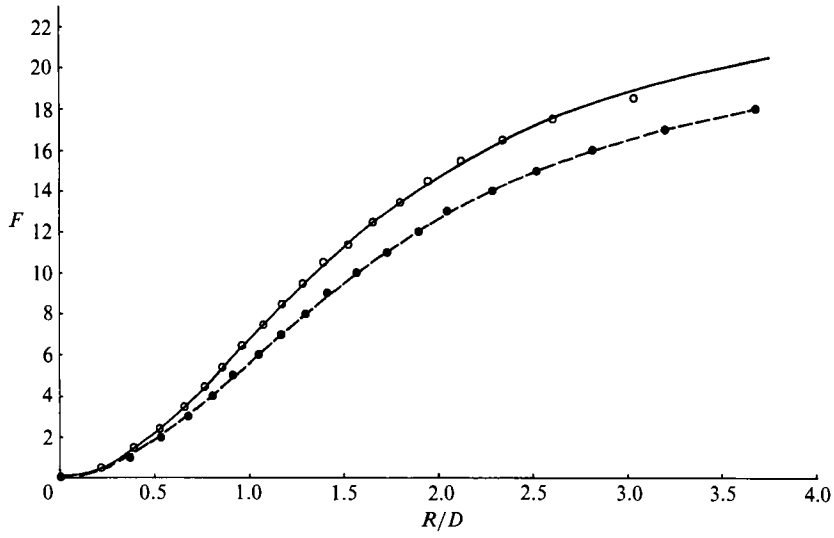

FIGURE 11. Matched experimental water surface profiles at $x/D = 10.8$ and 13.5 at $Re = 84.1$. The symbols represent the experimental measurements of the water surface profile, while the curves are from the Oseen-vortex water surface profile calculations using the measured surface tension. $D = 2.44$ mm.

(ii) For a given vortex age, the strength to make a theoretical profile pass through the first point was found.

(iii) If this theoretical profile did not come near to the second experimental point within a specifiable error then the age was altered accordingly and step (ii) was repeated. If the theoretical profile approached the second point to within a satisfactory degree then the match between the whole theoretical profile and the whole experimental profile was checked. If this was unsatisfactory, then two further points were chosen and the whole process was repeated. If the whole match was satisfactory, then the age and strength of the theoretical profile was taken as the age and strength of the shed vortex. Because of the different effects of age and strength on the water surface depression, unique results can be obtained.

When matching successive vortices in a vortex street, criteria such as monotonically increasing age and changes in maximum depression between vortices could be used to check the validity of a match. The accuracy of this method can be estimated by the range of ages and strengths that can give satisfactory matches – when combined with experimental error (which is essentially due to vibrations) the accuracy of the age is poor at typically 15%, though the accuracy of the strength is better than 5%. The method of analysis was such that if the age was calculated to be too high then the strength would also be too high.

6.1. *Variation with downstream distance*

Figure 11 shows the water surface profiles produced by Oseen vortices matched by the above method to the experimental profiles from figure 10 at $x/D = 10.8$ and 13.5 (x is measured from the back of the cylinder). It is important that the match is good where the water surface gradient is steep, since there the effect of inaccuracies caused by surface waves is going to be smallest. With the precautions taken, disturbance effects are judged to produce an error of one fringe. The slight departure at high R/D

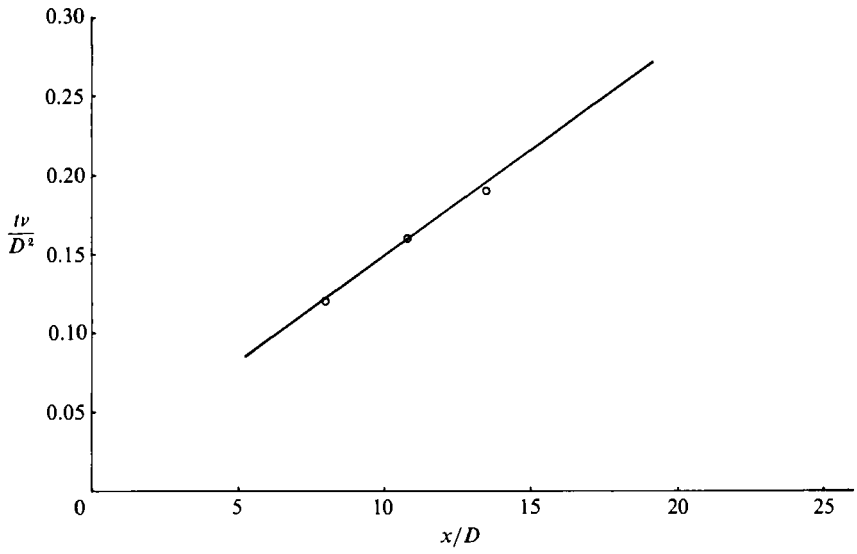

FIGURE 12. Variation of age along the wake at $Re = 84.1$. The symbols represent values of age calculated using the profile matching technique, while the solid line shows an increase in age of one period per wavelength, which is used to determine strength where the profile matching technique fails. $D = 2.44$ mm.

in the match for the profile at $x/D = 10.8$ is therefore judged to be of small significance when compared with the behaviour of the rest of the profile match. The properties of three vortices shed by a cylinder at $Re = 84.1$ are then as follows:

at $x/D = 8$, $K/\pi UD = 0.88$ and $tv/D^2 = 0.12$;

at $x/D = 10.8$, $K/\pi UD = 0.89$ and $tv/D^2 = 0.16$;

at $x/D = 13.5$, $K/\pi UD = 0.89$ and $tv/D^2 = 0.19$.

The average change in tv/D^2 between the above three shed vortices is 0.035. This figure agrees well with the half-period of shedding of 0.037 measured for this run, as one would expect.

No satisfactory match could be obtained for the vortex at $x/D = 5.2$. This is probably due to the distortion of the fringes caused by the dimple just behind the cylinder. Similar problems were encountered when trying to find matches for the vortices from $x/D = 16$ onwards owing to the now small number of fringes and much smaller water surface gradients. However, arguments such as monotonically increasing age and decreasing depth along the wake can be used to produce less accurate matches in these regions. The interaction of the vorticity regions of neighbouring vortices will eventually cause departures from the Oseen profile. It is possible that this is becoming noticeable at $x/D = 16$. The variation of age along the street is principally determined by the shedding period; the ages of two consecutive vortices should then differ by half a shedding period or less. In fact, the difference in age between the vortices at $x/D = 8$, 10.8 and 13 is about half a shedding period. Using this result the ages of vortices at other positions in the wake can be found by extrapolation, the difference in age between successive vortices being half a shedding period. This is the same as the relationship assumed by Schaefer & Eskinazi (1959) in their calculation of vortex strength. The variation of age with x/D is shown in figure 12; for the extrapolated age, the age at $x/D = 10.8$ is taken as the reference value and the variation of age (the gradient of the line) is one shedding period per

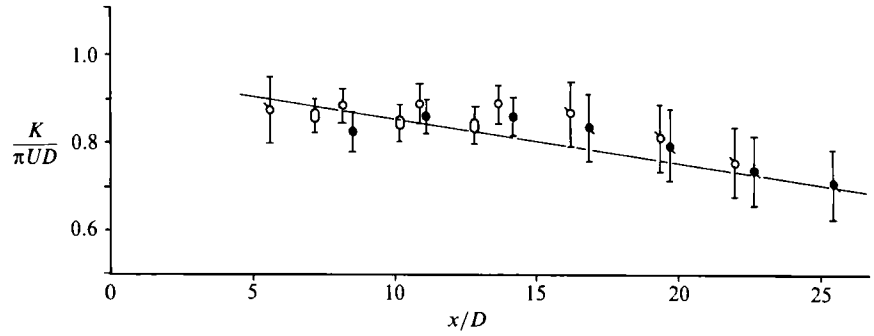

FIGURE 13. Variation of dimensionless strength along the wake at $Re = 80$. The flagged symbols represent vortex strengths calculated where profile matching has failed (age extrapolation). 0, $Re = 80.3$, $D = 3.02$ mm; ●, $Re = 81.7$, $D = 2.44$ mm; ○, $Re = 84.1$, $D = 2.44$ mm. The line drawn represents 1% decrease per unit x/D.

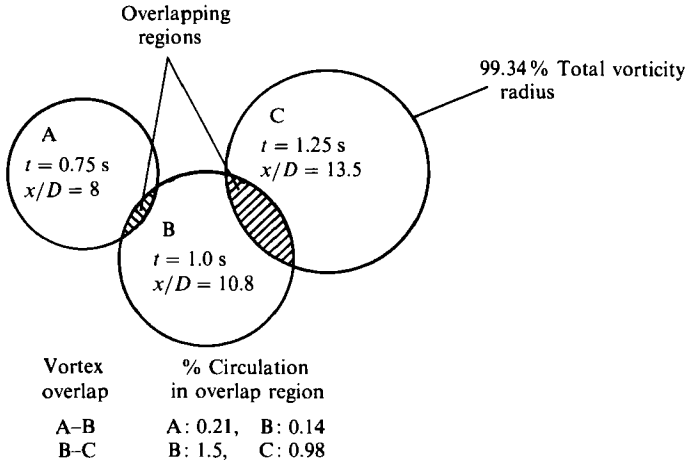

FIGURE 14. Simple wake model to illustrate vortex weakening. The amount of circulation of each vortex contained in the overlap region is indicated.

wavelength. Since the maximum depressions of these vortices are known, then values of the strength can be found. The surface profile corresponding to the calculated age and strength is then compared with the experimental profile so that the errors can be assessed. These were determined from the pairs of values of strength and age which could produce the observed central depression. Vortex strengths calculated in this way are less accurate (typically 8–9%) than those found by the profile matching technique (at worst 5%). The variation in strength along the wake is shown in figure 13 with error bars corresponding to the values above. The agreement of results obtained at the same Reynolds number from cylinders of different diameter substantiates the method.

The fall in strength with downstream distance is significant. Flow visualization of vortex streets shows that they widen with downstream distance beyond x/D values of 2–4 (see e.g. Batchelor 1967). This observed widening can be accounted for by the transverse velocity induced by a weakening of the vortices, due to overlapping of the

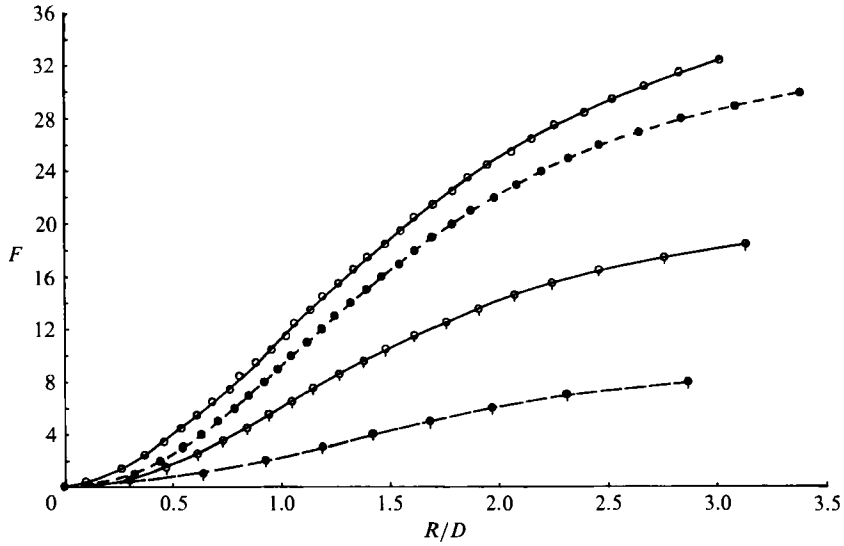

FIGURE 15. Effect of Re on water surface profile at $x/D = 10$ below $Re = 102$. $D = 2.44$ mm. ⚲, $Re = 67.4$; ⚲, $Re = 81.7$; ●, $Re = 91.0$; ○, $Re = 95.1$.

vortex cores and thus cancellation of vorticity, of about 1% for each unit of x/D. This line is drawn on figure 13. The vortex strengths and ages that we have presented correspond to overlapping vortex cores as shown in figure 14. The shaded regions contain oppositely signed vorticity, the amount of circulation from each vortex contained in each region being indicated. Since the periods of rotation of the edges of the circles containing 99.34% of the circulation are large (5.3, 7 and 8 shedding periods for vortices A, B and C respectively) the cancellation of vorticity in the range $8 < x/D < 13.5$ is essentially limited to the shaded regions. Though very little vorticity is convected into these regions diffusion into the region of cancellation is increased.

6.2. *Variation with Reynolds number*

As Reynolds number increased, the variation of vortex strength along the wake followed a similar pattern to that discussed in the last section. The value of x/D at which the strength began to fall, however, increased slowly with Reynolds number. No basic change in the appearance of the shedding cycle was observed as the Reynolds number increased. Figure 15 shows the change in water surface profile for the range $67.4 < Re < 95.1$ for a cylinder diameter of 2.44 mm. As can be seen, the water surface height above the vortex centre at given R/D increases considerably with Re. This change is almost entirely due to increase in vortex strength: the ages of the vortices at a given x/D are almost constant in this range of Reynolds number. Figure 16 shows the variation of the dimensionless vortex strength with Reynolds number found by profile matching to an accuracy of within 5%. The straight line drawn on the figure is close to $K/\pi UD$ being proportional to Re. The slope is 16% higher than the directly proportional line and intersects $K/\pi UD = 0$ at $Re = 12.9$. The change in strength at $Re = 102$ is quite sudden, the value of the dimensionless strength at $Re = 122.8$ is about 34% less than it would have been without the change. The strength measurements shown in figure 16 are also shown in figure 1 where it can be seen that the agreement with the other determinations of vortex

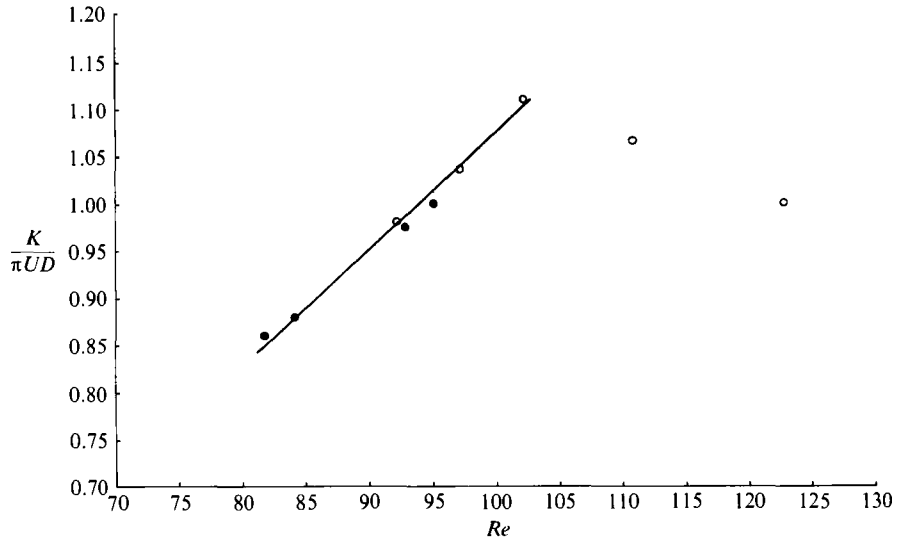

FIGURE 16. Variation of dimensionless vortex strength with Re found using the profile matching technique. This holds in the constant-strength region of the wake ($5 < x/D < 16$). The solid line has been fitted to the measured vortex strengths and deviates slightly from $K/\pi UD \propto Re$. ○, $D = 3.02$ mm; ●, $D = 2.44$ mm.

strength is quite good. The age at $x/D = 10$ below $Re = 102$ is almost constant; however, by examining the position of maximum water surface gradient and using the technique of profile matching, it was found that the age starts to decrease above $Re = 102$, the value at $Re = 122.8$ being some 15% lower than at $Re = 102.2$. The decrease in age signifies an increase in concentration of vorticity.

7. Further experiments and discussion

In view of the protracted discussion on the discontinuities in the Strouhal number – Reynolds number relationship, which have finally been attributed by Williamson (1989) to three-dimensional effects, some remarks on these effects in the present experiments are necessary. Preliminary flow visualization of the wake showed parallel shedding in the range of Reynolds number covered in this paper. The observations were made with the cylinder supported above the water surface and extending almost to the bottom of the tank (no U-shaped cradle) and before the honeycomb was inserted. The effective aspect ratio of the cylinders was 102 and 128. The major source of three-dimensionality was the existence of a boundary layer on the lower plate of the cradle. Vortex lines must, however, approach the water surface normally (at the centre of the effective cylinder length). In addition to the flow over the cradle distorting the vortices, pressure changes over the cradle will cause small water surface deformations. By running the cradle through the water tank without a cylinder model attached, it was found that the water surface deformation caused by the cradle itself amounted to about one fringe over the region of the field of view of interest (i.e. over $5D$ either side of the wake). To test for the effect of three-dimensional shedding itself, the wake of a cylinder model with the diameter of the lower half of the cylinder span twice that of the upper half was studied. This arrangement and diameter ratio was exactly that studied (later) by Eisenlohr &

Eckelmann (1989). When compared with the wake of a two-dimensional cylinder, the vortex paths at the surface were seen to be highly distorted. Vortex paths behind a two-dimensional cylinder were usually seen to diverge from the wake centreline up to at least $x/D = 20$ (x is measured from the back of the cylinder). The vortex paths behind the three-dimensional cylinder followed no such easily describable pattern, the wake centreline being itself highly distorted. However, the water surface profiles for the three-dimensional cylinder were found to disagree with profiles for two-dimensional cylinders by no more than one fringe, which is as good as the expected accuracy. This means that gross three-dimensional distortion sufficiently far below the water surface has a negligible effect on the water surface deformation caused by individual vortices. Since the shed vortices must approach the water surface normally and, therefore, a small region of two-dimensionality exists, it is likely that the interferograms accurately represent the water surface deformation caused by a two-dimensional cylinder. Calculations using the Biot–Savart law show that, at a distance of 2 D from the vortex axis, the velocity induced at the water surface by a vortex (and its image in the water surface) shed by a cylinder of aspect ratio 14 is only 1 % less than the induced velocity produced by a vortex from an infinite cylinder. This is equivalent to about half a fringe out of 25.

The existence of transition at $Re \approx 100$ has been confirmed by the present results. The variation of the vortex strength with Reynolds number has shown that there is a change in the manner in which the shed vortex strength is determined at $Re \approx 100$ even though the interferograms showed no radical change in the appearance of the wake. Flow visualization by Slaouti (1980) showed a clear change in the residence time of marked liquid in the region close behind the cylinder at $Re = 100$. This change, also seen in the work of Freymuth *et al.* (1986), is that the entrainment of fluid into the shear layers rolling up into vortices is considerably more energetic as Re increases beyond 100. This is connected with the amount by which the shed vortex strength is less than the circulation, Γ, shed in one periodic time from one side of the cylinder. The circulation Γ generated in a boundary layer on one side of the cylinder over one shedding cycle is given by $\Gamma \approx \frac{1}{2}U_s{}^2T$ where U_s is the mean velocity at the edge of the boundary layer at separation and T is the shedding period. The proportion of the circulation lost is then given by $(1-K/\Gamma)$. Figure 17 shows the change in percentage loss in circulation with Reynolds number. The shedding period was measured from the interferograms whilst the separation velocity was abstracted from Grove *et al.* (1964). The circulation loss decreases continuously with Re up to $Re = 100$ and remains roughly constant thereafter at about 32 %. The decreases up to $Re \approx 100$ reflects the diminishing role of the main mechanism for destruction of vorticity in that Reynolds number range, whilst the behaviour after $Re = 100$ shows that some new mechanism has appeared. The circulation shed from the separation line increases steadily as Re increases from 50 to 170 (Williamson & Roshko 1990) if we assume that $U_s/U = 1-C_{p_b}$. The Strouhal number increases similarly. Williamson & Roshko call these 'mean quantities', as is the Reynolds number itself. The Reynolds number is a measure of the ratio of rate of convection of vorticity to the rate of diffusion of vorticity. Whilst the mean quantities show a smooth increase there is a continuous change in the vorticity distribution. Not only does the vortex strength change but its spatial distribution changes from being spread in the streamwise direction to being more concentrated at higher Reynolds numbers. The onset of appreciable cross-flow in the near wake increases the entrainment of oppositely signed vorticity and also produces this at the rear surface of the body. This reorganization of the vorticity distribution appears to be the start of the

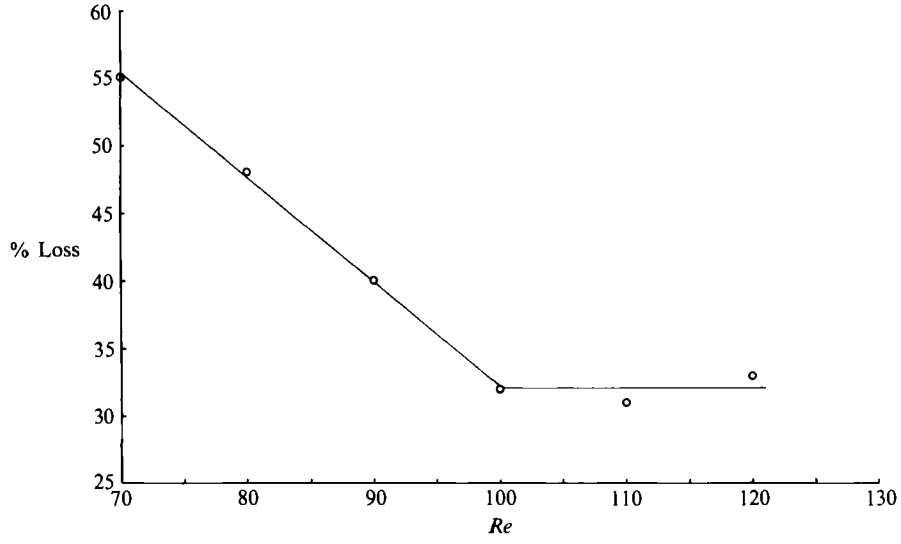

FIGURE 17. Change of proportion of loss of circulation with Re. Loss of circulation is $1\text{-}K/\Gamma$, where K is the vortex strength and Γ is the boundary-layer circulation shed from one side of cylinder in one shedding period.

shedding mechanism postulated by Gerrard (1966). Why the rate of change of shed vortex strength with Reynolds number should be discontinuous is unexplained.

8. Conclusions

Vortex strengths in the wakes of cylinders of aspect ratio greater than 100 have been determined to an accuracy of better than $\pm 5\%$ where profile matching was possible. Values determined using extrapolated ages were determined to better than $\pm 9\%$. The vortex surface depressions of the vortices at distances downstream of the cylinder greater than $5D$ were shown to possess Oseen vortex distributions. The starting point of the investigation illustrated in figure 1 showed a possible sharp discontinuity at $Re = 100$ from the results of different workers and with unknown accuracy. We have observed the discontinuity in vortex strengths in a single experiment. The change at $Re = 100$ is not connected with three-dimensional effects and so also not with discontinuities in the Strouhal number–Reynolds number relationship which have been the subject of much discussion. The transition is associated with a change in the orientation of the near-wake vorticity, with an increase in cross-flow behind the cylinder and with increased entrainment into the separated shear layers rolling up into vortices. The reason for the discontinuous nature of the transition is unexplained.

There remains a great deal to be discovered about bluff-body wakes at low Reynolds number. Our determinations of vortex strength from integration of the vorticity field (Green 1989) reveal further changes at slightly higher Reynolds numbers. These concur with the oscillating velocity results of Unal & Rockwell (1988) who find a maximum at $Re \approx 200$ (where the base suction peaks). Their results do not show a decrease just beyond $Re \approx 100$, which also invites explanation.

REFERENCES

BATCHELOR, G. K. 1967 *An Introduction to Fluid Dynamics*. Cambridge University Press.

BENSON, M. G., BELLAMY-KNIGHTS, P. G., GERRARD, J. H. & GLADWELL, I. 1989 A viscous splitting algorithm applied to low Reynolds number flow around a circular cylinder. *J. Fluids Struct.* **3**, 439.

BERGER, E. 1964 The determination of the hydrodynamic parameters of a Karman vortex street from hot wire measurements at low Reynolds numbers. *Z. Flugwiss.* **12**, 41.

BLOOR, M. S. & GERRARD, J. H. 1966 Measurements on turbulent vortices in a cylinder wake. *Proc. R. Soc. Lond.* A **294**, 319.

BRAZA, M., CHASSAING, P. & HA MINH, H. 1986 Numerical study and physical analysis of the pressure and velocity fields in the near wake of a cylinder. *J. Fluid Mech.* **165**, 79.

CIMBALA, J. M., NAGIB, H. M. & ROSHKO, A. 1988 Large structure in the far wakes of two-dimensional bluff bodies. *J. Fluid Mech.* **190**, 265.

DALY, B. J. 1969 A technique for including surface tension effects in hydrodynamic calculations. *J. Comput. Phys.* **4**, 97.

EISENLOHR, H. & ECKELMANN, H. 1989 Vortex splitting and its consequences in the vortex street wake of cylinders at low Reynolds number. *Phys. Fluids* A **1**, 189.

EISNER, F. 1929 Drag measurements on towed cylinders of circular and bridge pile cross sections. Mitteilungen der Preussischen Versuchsanhalt fuer Wasser und Schiffbau, Berlin. **4**, 1.

FREYMUTH, P., FINAISH, F. & BANK, W. 1986 Visualisation of the vortex street behind a circular cylinder at low Reynolds number. *Phys. Fluids* **29**, 1321.

GASTER, M. 1971 Vortex shedding from circular cylinders at low Reynolds numbers. *J. Fluid Mech.* **46**, 749.

GERRARD, J. H. 1966 The mechanics of the formation region of vortices behind bluff bodies. *J. Fluid Mech.* **25**, 401.

GERRARD, J. H. 1978 The wakes of cylindrical bluff bodies at low Reynolds numbers. *Phil. Trans. R. Soc. Lond.* A **288**, 351.

GREEN, R. B. 1989 Measurement of vorticity and vortex strength in the wake of a circular cylinder at low Reynolds number. Ph.D. thesis, University of Manchester.

GROVE, A. S., SHAIR, F. M., PETERSEN, E. E. & ACRIVOS, A. 1964 An experimental investigation of the steady separated flow past a circular cylinder. *J. Fluid Mech.* **19**, 60.

HONJI, H. 1986 Downstream persistence of regular vortex streets. *J. Phys. Soc. Japan* **55**, 2897.

MARSTON, P. L. & FAIRBANK, M. F. 1977 Evidence of a large superfluid vortex in He II. *Phys. Rev. Lett.* **39**, 1208.

ROSHKO, A. 1954 On the drag and shedding frequency of two dimensional bluff bodies. *NACA Tech. Note* 3169.

SCHAEFER, J. W. & ESKINAZI, S. 1959 An analysis of the vortex street generated in a viscous fluid. *J. Fluid Mech.* **6**, 241.

SCHMIDT, D. W. & TILMAN, P. M. 1972 On the vortex strength of circular cylinder wakes. *Acustica* **27**, 14.

SLAOUTI, A. 1980 The oscillating wake behind a circular cylinder at low Reynolds numbers. Ph.D. thesis, University of Manchester.

SLAOUTI, A. & GERRARD, J. H. 1981 An experimental investigation of the end effects on the wake of a cylinder towed through water at low Reynolds number. *J. Fluid Mech.* **112**, 297.

TANEDA, S. 1959 Downstream development of wakes behind cylinders. *J. Phys. Soc. Japan* **14**, 843.

TANIDA, Y., OKAJIMA, A. & WATANABE, Y. 1973 Stability of a circular cylinder oscillating in uniform flow or in a wake. *J. Fluid Mech.* **61**, 769.

THOM, A. 1933 The flow past circular cylinders at low speeds. *Proc. R. Soc. Lond.* A **141**, 651.

TIMME, A. 1957 On the velocity distribution in vortices. *Ing. Arch.* **25**, 205.

TRITTON, D. J. 1959 Experiments on the flow past circular cylinders at low Reynolds number. *J. Fluid Mech.* **6**, 547.

UNAL, M. F. & ROCKWELL, D. 1988 On vortex formation from a cylinder Part I. The initial instability. *J. Fluid Mech.* **190**, 491.

WILLIAMSON, C. M. K. 1988 The existence of two stages in the transition to three-dimensionality of a cylinder wake. *Phys. Fluids* **31**, 3165.

WILLIAMSON, C. M. K. 1989 Oblique and parallel modes of vortex shedding in the wake of a circular cylinder at low Reynolds numbers. *J. Fluid Mech.* **206**, 579.

WILLIAMSON, C. M. K. & ROSHKO, A. 1990 Measurements of base pressure in the wake of a cylinder at low Reynolds number. *Z. Flugwiss. Weltraumforsch.* **14**, 38.

ZDRAVKOVICH, M. M. 1969 Smoke observations of the formation of a Karman vortex street. *J. Fluid Mech.* **37**, 491.